Viser Technology Pte. Ltd.
Research and Application of Materials Science
DOI: 10.33142/rams.v7i2.19667

Research Article Open Access

Carbonized Polymer Dots-Induced Multivalent Hydrogen-Bonding Networks in Hydrogel Electrolytes for High-Performance Low-Temperature Zinc-Ion Batteries

Yuming LIU[†], Xin JI[†], Siyu ZHANG, Yangyu SUN, Haizhu SUN[*]

Key Laboratory of Sustained and Advanced Functional Materials, College of Chemistry, Northeast Normal University, Changchun Jilin 130024, P. R. China

[*]***Corresponding Author:*** *Haizhu SUN, E-mail: sunhz335@nenu.edu.cn*
[†]***Co-first Authors:*** *Yuming LIU and Xin JI*

Abstract

Aqueous zinc-ion batteries (AZIBs) are considered promising candidates for next-generation energy storage systems owing to their intrinsic safety, low cost, high theoretical capacity (820 mAh g^{-1}), and environmental friendliness. However, the excessive free water in conventional aqueous electrolytes severely compromises low-temperature performance due to the inherently high freezing point of water. Moreover, water-induced parasitic reactions on the Zn metal anode, including hydrogen evolution, corrosion, and passivation, inevitably lead to poor electrode reversibility and limited cycling stability, thereby hindering their practical applications in low-temperature environments. Herein, carbonized polymer dots (CPDs) with abundant surface functional groups are introduced to regulate the hydrogen-bonding environment within the hydrogel electrolyte. The CPDs effectively disrupt the original hydrogen-bonding network of free water and reconstruct multivalent hydrogen-bonding interactions among CPDs, free water, and polyacrylamide (PAM) chains. Such a strategy immobilizes free water and converts it into bound water, thereby significantly depressing the freezing point of the electrolyte. In addition, CPDs facilitate rapid Zn^{2+} transport under low-temperature conditions while simultaneously suppressing Zn dendrite growth and undesirable side reactions. Furthermore, the influence of CPDs content on the electrochemical performance was systematically investigated by tuning the volume ratio between CPDs and PAM. When the CPDs volume ratio reached 0.3, the Zn||Zn symmetric cell exhibited highly stable cycling performance for 800 h (2 mA $cm^{-2,}$ 1 mAh cm^{-2}) at -25°C. This work provides a feasible strategy for the rational design of high-performance low-temperature resistance hydrogel electrolytes for advanced zinc-ion batteries.

Keywords: *Carbonized polymer dots (CPDs); polyacrylamide (PAM); low-temperature resistance*

1 Introduction

Currently, aqueous zinc-ion batteries (AZIBs) have attracted extensive attention owing to their high safety, environmental benignity, and high energy density [1-4]. However, several critical challenges, including uncontrolled zinc dendrite growth, hydrogen evolution reactions, corrosion, and internal short circuits, still severely hinder their practical applications and cycling stability [5-8]. Although gel electrolytes can effectively suppress electrolyte leakage and reduce the risk of internal short circuits, issues associated with sluggish ion transport and insufficient inhibition of zinc dendrites remain unresolved [9,10].

To address these limitations, various strategies have been proposed, including the construction of composite electrodes, the introduction of electrolyte additives, and the development of composite gel electrolytes [11]. Among these approaches, composite gel electrolytes have attracted considerable interest because of their high thermal stability, excellent electrode/electrolyte interfacial contact, and enhanced ionic conductivity derived from improved ion transport kinetics [12,13]. For example, Zhuang et al. developed an acidic PAMPS/PAM hydrogel electrolyte in which abundant sulfonic acid groups acted as proton reservoirs to maintain a stable acidic environment and facilitate cation transport [14]. In another study, Wan and co-workers fabricated TPU/PVA composite gel electrolytes through solution blending and phase inversion methods, where the formation of a semi-interpenetrating polymer network synergistically enhanced mechanical stability and ion transport capability. Furthermore, hydrogen-bonding interactions between abundant polar groups and hydrogen ions effectively reduced free proton activity, thereby suppressing zinc dendrite growth and

Received: October 30, 2025; Accepted: December 18, 2025

electrode corrosion while maintaining high ionic conductivity [15]. Nevertheless, current studies on AZIBs capable of simultaneously achieving high energy density and long-term cycling stability under low-temperature conditions remain limited, highlighting the urgent need for efficient Low-Temperature gel electrolytes [16].

Polyacrylamide (PAM) has been widely employed as a gel electrolyte matrix because of its low cost, facile fabrication process, and favorable ionic transport properties. Its three-dimensional polymer network promotes the homogeneous distribution of Zn^{2+} while maintaining good ionic conductivity. However, the intrinsic antifreezing capability of PAM remains inadequate, and its relatively weak mechanical strength cannot effectively suppress zinc dendrite growth during prolonged cycling [17,18]. In this context, carbonized polymer dots (CPDs), as an emerging class of zero-dimensional carbon-based nanomaterials, offer new opportunities for the design of advanced low-temperature gel electrolytes. CPDs possess a carbonaceous core enriched with abundant tunable surface-active sites and excellent dispersibility. More importantly, the abundant oxygen-containing functional groups on CPDs can reconstruct hydrogen-bonding interactions within the electrolyte and regulate Zn^{2+} deposition behavior, thereby enabling more uniform zinc plating/stripping processes and improved electrochemical stability under low-temperature conditions [19].

Herein, a composite hydrogel electrolyte based on polyacrylamide (PAM) and carbonized polymer dots (CPDs) was constructed, as illustrated in Figure 1. The CPDs, derived from glucose and ethanol, are enriched with abundant hydroxyl and carboxyl functional groups, which can effectively disrupt the original hydrogen-bonding network of free water. Through the synergistic interactions among CPDs, PAM chains, and water molecules, a multivalent hydrogen-bonding network is reconstructed within the electrolyte, thereby immobilizing free water and converting it into bound water to reduce the freezing point of the electrolyte [20,21]. Meanwhile, the reconstructed hydrogen-bonding environment effectively regulates the Zn^{2+} solvation structure and facilitates rapid Zn^{2+} transport under low-temperature conditions, resulting in more uniform Zn deposition behavior and suppressed zinc dendrite growth as well as parasitic side reactions [22]. Furthermore, the influence of CPDs content on the electrochemical performance was systematically investigated to determine the optimal composition. Benefiting from the optimized hydrogen-bonding network and enhanced ion transport behavior, the assembled Zn||Zn symmetric cell with the optimized gel electrolyte achieved stable cycling performance for 800 h at -25 ℃ under a current density of 2 mA cm^{-2} and an areal capacity of 1 mAh cm^{-2}. This work provides an effective strategy for the rational design of high-performance low-temperature hydrogel electrolytes for advanced aqueous zinc-ion batteries.

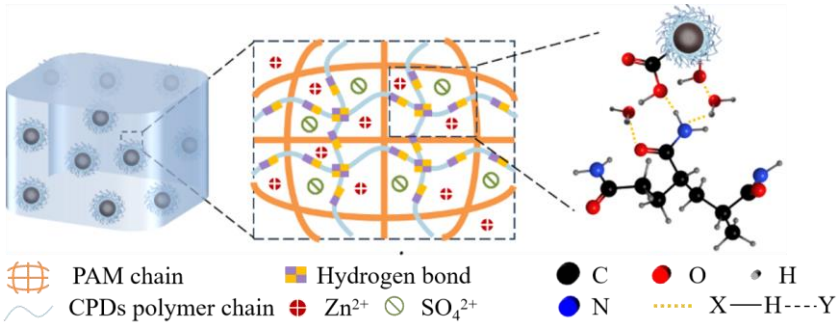

Figure 1 Specific schematic diagram of the PAM-CPDs

2 Experiment Section

2.1 Preparation of CPDs

0.75 g of glucose was weighed and dissolved in 60 mL of ethanol. The mixture was stirred at room temperature for ten minutes, and then the resulting solution was transferred to a sealed high-pressure reactor lined with polytetrafluoroethylene (PTFE). The solvothermal reaction was conducted under high pressure at 180 ℃ for 12 h. After cooling to room temperature, the solution containing CPDs was obtained.

2.2 Preparation of hydrogel

The synthesis was carried out with volume ratios of aqueous solution to carbon dot solution of 10:0, 9:1, 7:3, 5:5, and 3:7. For each ratio, 5.7512 g of $ZnSO_4 \cdot 7H_2O$was added to the corresponding volume of purified water (10 mL, 9 mL, 7 mL, 5 mL, and 3 mL, respectively), and the mixtures were stirred at room temperature.

Subsequently, the carbon dot solution was added in the specified proportions, along with 2 g of AM (acrylamide monomer) and 2.5 mg of MBAA (N, N'-methylenebisacrylamide, the crosslinker). After the mixture was stirred for 30 minutes at room temperature, APS (ammonium persulfate, the initiator) was added, and stirring was continued until all solids were dissolved. The stirred solution was then poured into the gap of a glass plate secured with clamps and was reacted at 60 ℃ for 2 h to obtain the desired gel. The gel thickness was

determined by the glass plate gap; a thickness of 1 mm was obtained, with a measurement error not exceeding 0.01 mm. The synthesized gel was subsequently pressed into uniformly sized discs with a diameter of 15.8 mm using a presser.

2.2.1 Assembly of cells

The coin-shaped CR2032 Zn||Zn symmetric battery is fabricated from two zinc foils and a gel electrolyte containing different PAM-CPDs formulations.

2.2.2 Types of instruments and tests

The characteristic functional groups in CPDs electrolytes with varying concentrations were characterized using an Agilent Technologies Cray 630 FTIR (Fourier Transform Infrared) spectrometer; Raman spectroscopy was employed to characterize the surface functional groups in CPDs electrolytes with different concentrations. Electrochemical impedance spectroscopy (EIS) measurements were performed using the CHI660E electrochemical workstation, with an amplitude of 5 mV and a frequency range from 10^{-2} Hz to 10^{6} Hz. The hydrogen evolution reaction (HER) was investigated by linear scanning voltammetry (LSV) at a scanning rate of 1 mV s^{-1}, within the scanning ranges of 0 to -0.5 V and 0 to 3 V.

3 Results and discussion

3.1 Structure characterization of CPDs

First, the gel electrolyte additive CPDs were characterized. As shown in Fig. 2a, the CPDs solution exhibits a uniformly dispersed deep brown color. Under 365 nm ultraviolet irradiation (Fig. 2b), the CPDs solution displays bright blue fluorescence, demonstrating the excellent fluorescent properties of the synthesized CPDs. To investigate the structure and morphology of CPDs, XRD analysis was first conducted. As shown in Fig. 2c, a broad diffraction peak centered at approximately 25 ° is observed, which can be attributed to amorphous carbon, indicating that the CPDs consist of carbonized polymer dots with carbon nuclei as the core structure. To further identify the surface functional groups of the CPDs, FT-IR and XPS analyses were subsequently performed. As shown in Fig. 2d, characteristic absorption peaks corresponding to O-H, C=O, C=C, and C-O-C functional groups are clearly observed, confirming the successful introduction of abundant oxygen-containing functional groups onto the CPDs surface. Furthermore, XPS measurements were carried out to further verify the surface chemical composition and bonding states of the CPDs. The high-resolution C 1s spectrum shown in Fig. 2f can be deconvoluted into four characteristic peaks corresponding to C-C/C-H (284 eV), C-O-C (286 eV), O=C-O (289 eV), and -OH (291 eV), respectively. Meanwhile, the high-resolution O 1s spectrum in Fig. 2g reveals characteristic peaks attributed to C-O (532 eV), O=C-O (533 eV), and -OH (535 eV), which is consistent with the FT-IR results. The above results demonstrate that CPDs with a carbon core and surfaces rich in oxygen-containing functional groups, such as -OH and -COOH, were successfully synthesized. These abundant surface functional groups can effectively disrupt the hydrogen-bonding interactions of free water and further establish multiple hydrogen-bonding interactions with both water molecules in the hydrogel electrolyte and PAM polymer chains. Consequently, the proportion of bound water is increased, thereby enhancing the low-temperature adaptability of the hydrogel electrolyte.

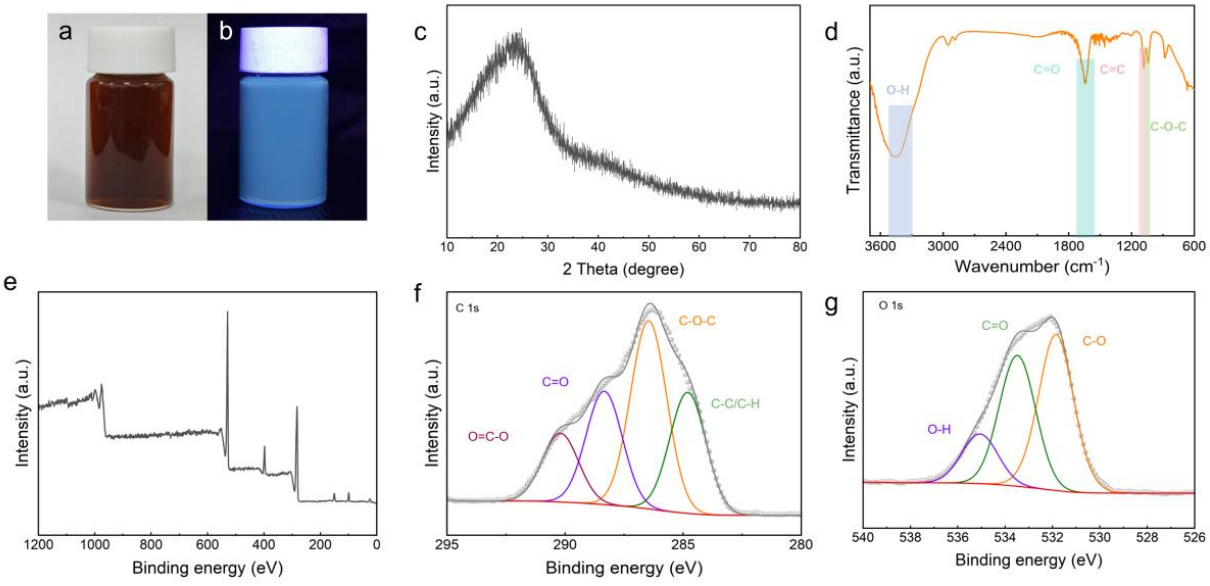

Figure 2 (a-b) Photographs of the CPDs solution under visible light and 365 nm UV irradiation, respectively. (c) XRD pattern of CPDs. (d) FT-IR spectrum of CPDs. (e) XPS survey spectrum of CPDs. High-resolution XPS spectra of (f) C 1s and (g) O 1s for CPDs.

3.2 Morphology of PAM-CPDs gel electrolytes

As shown in Fig. 3a, the AM precursor solution was initially colorless and transparent before polymerization at room temperature. With the gradual increase in the volume ratio of the CPDs solution, the color of the precursor solution progressively deepened and became increasingly brown. Subsequently, the precursor solution was polymerized at 60 ℃ for 2 h. After polymerization, the obtained electrolyte remained stable regardless of bottle inclination, confirming the successful formation of the gel electrolyte. After storage at -25 ℃ for 2 h, the pure PAM electrolyte transformed into a white opaque solid. This phenomenon was mainly attributed to the precipitation of $ZnSO_4$ crystals at low temperatures, which severely hindered ion transport within the electrolyte. In contrast, freezing was no longer observed in the PAM-0.3CPDs, PAM-0.5CPDs, and PAM-0.7CPDs gel electrolytes with increasing CPDs content, indicating that the incorporation of CPDs effectively enhanced the structural stability and low-temperature adaptability of the gel electrolyte. As shown in Fig. 3b, the synthesized gel electrolytes were cut into circular discs with a diameter of approximately 15.8 mm (error ≤ 0.1 mm) and an initial thickness of 1 mm. The detailed thickness measurements are presented in Fig. 3c. Considering that the thickness of the external protective film was 0.066 mm, the actual thicknesses of the gel electrolytes were calculated to be 0.855, 0.851, 0.854, 0.852, and 0.753 mm, respectively. However, when the CPDs content reached 70%, the gel electrolyte exhibited obvious deformation and could no longer be pressed into a regular circular sheet. This result indicates that excessive CPDs significantly increased the viscosity of the PAM hydrogel electrolyte, thereby hindering Zn^{2+} transport within the electrolyte network.

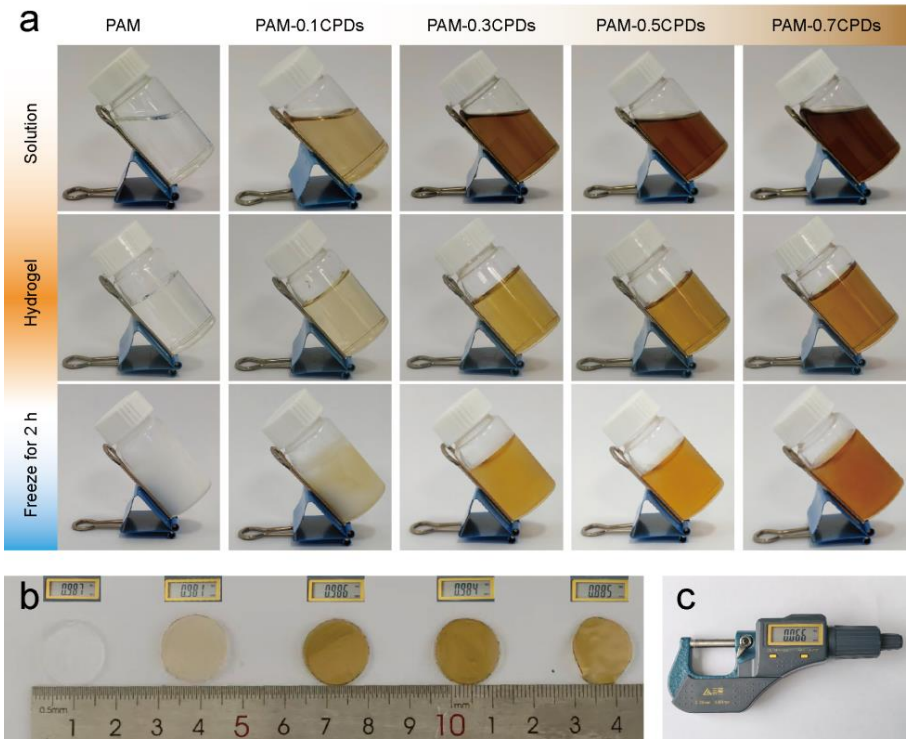

Figure 3 (a) Photos of the synthesized material under room temperature, heated, and frozen conditions; (b) Photos of the diameter of the gel electrolyte; (c) Thickness of the film outside the gel electrolyte (single layer). Supplementary thickness diagrams for each gel electrolyte are embedded in (b).

3.3 Structure PAM-CPDs gel electrolytes

As shown in Fig. 4a, the freezing points of pure PAM, PAM-0.1CPDs, PAM-0.3CPDs, and PAM-0.5CPDs are -9.5 ℃, -14.84 ℃, -20.33 ℃, and -26.85 ℃, respectively. These results demonstrate that the freezing point of the PAM–CPDs composite gel electrolyte gradually decreases with increasing CPDs content. Compared with pure PAM, the composite gel electrolytes exhibit significantly enhanced low-temperature adaptability, which is consistent with the observations shown in Fig. 3a. As shown in the FT-IR spectra in Fig. 4b, the absorption peaks in the range of 3300-3200 cm^{-1} correspond to the stretching vibrations of O-H groups. With increasing CPDs content, the hydroxyl absorption peak gradually shifts toward lower wavenumbers, while the characteristic absorption peak located at 1700-1650 cm^{-1}, corresponding to the bending vibrations of water molecules, gradually shifts toward higher wavenumbers. These results indicate that the hydroxyl and carboxyl groups on CPDs effectively disrupt the hydrogen-bonding interactions of free water, thereby

promoting the formation of multiple hydrogen bonds among free water, PAM chains, and CPDs. As shown in Fig. 4c, the Raman spectra reveal that the intensities of the characteristic C-OH peak (1360-1450 cm^{-1}) and C-O peak (1150-1050 cm^{-1}) gradually increase with increasing CPDs content, confirming the successful introduction of abundant oxygen-containing functional groups by CPDs. Meanwhile, the C-C skeletal vibration peak (1000-950 cm^{-1}) exhibits gradual enhancement accompanied by a blue shift, while the -CH_2 bending vibration peak (900-800 cm^{-1}) also shows enhanced intensity and a blue shift. In addition, the C-C-O skeletal vibration peak (650-550 cm^{-1}) displays enhanced intensity together with a red shift. These results further demonstrate that multiple hydrogen-bonding interactions are formed among CPDs, PAM chains, and free water molecules. Consistent with the FT-IR results, these interactions provide the structural basis for the formation of a cross-linked network, thereby enhancing the overall performance and low-temperature stability of the gel electrolyte.

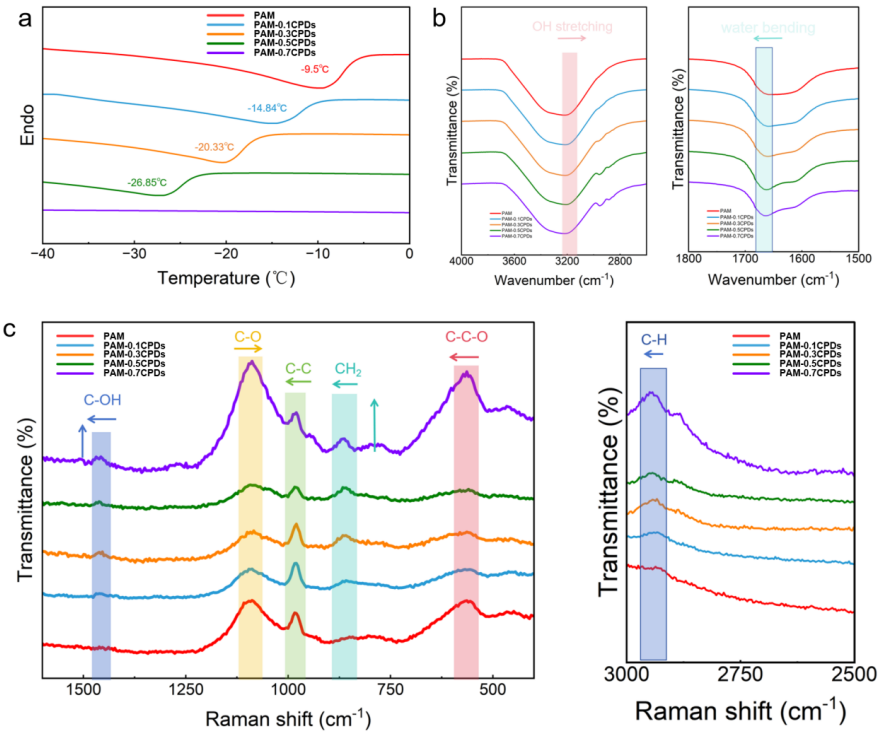

Figure 4 (a) DSC curves of the PAM, PAM-0.1CPDs, PAM-0.3CPDs, PAM-0.5CPDs, and PAM-0.7CPDs gel electrolytes; (b) Infrared spectroscopy spectra; (c) Raman spectroscopy spectra.

3.4 Electrochemical performance testing

To evaluate the electrochemical performance of the gel electrolytes and determine the optimal CPDs content, rate capability and long-term cycling tests were conducted using Zn||Zn symmetric cells. As shown in Fig. 5a, the rate performance was investigated at a fixed areal capacity of 1 mAh cm^{-2} while varying the current density from 0.1 to 10 mA cm^{-2}, followed by returning to 1 mA cm^{-2} for continuous cycling. The pure PAM electrolyte exhibited obvious voltage polarization, and the overpotential increased significantly during the middle and later stages of cycling. The total cycling durations of PAM, PAM-0.1CPDs, PAM-0.3CPDs, PAM-0.5CPDs, and PAM-0.7CPDs were 109 h, 75 h, 140 h, 143 h and 55 h, respectively. These results indicate that the introduction of CPDs effectively improves the electrochemical stability of the PAM electrolyte under varying current densities and reduces the risk of short-circuit failure. In particular, the PAM-0.3CPDs electrolyte exhibited the lowest overpotential, suggesting optimized Zn^{2+} transport kinetics and more stable Zn plating/stripping behavior. Long-term cycling tests were further performed at a fixed current density of 2 mA cm^{-2} and an areal capacity of 1 mAh cm^{-2}. As shown in Fig. 5b, at -5 ℃, the pure PAM electrolyte maintained stable cycling for only 200 h, whereas the cycling lifetimes of PAM-0.1CPDs, PAM-0.3CPDs, and PAM-0.5CPDs reached 346, 742, and 349 h, respectively. In contrast, PAM-0.7CPDs failed to sustain stable long-term cycling under the same conditions. Among all samples, PAM-0.3CPDs exhibited the longest cycling lifespan and the most stable electrochemical performance. Furthermore, as shown in Fig. 5d, when the temperature was decreased to -25 ℃, the pure PAM electrolyte solidified completely and lost its ionic conductivity. Under these conditions, the cycling lifetimes of PAM-0.1CPDs, PAM-0.3CPDs, and PAM-0.5CPDs were

6 h, 800 h and 186 h, respectively, whereas neither PAM nor PAM-0.7CPDs could maintain stable cycling. These results further confirm that the optimized hydrogen-bonding network induced by CPDs effectively enhances the low-temperature adaptability and interfacial stability of the hydrogel electrolyte.

3.5 Investigation of electrolyte properties

First, linear sweep voltammetry (LSV) was employed to evaluate the electrochemical stability window of the gel electrolytes during the charging/discharging process. As shown in Fig. 6a, the PAM and PAM-0.7CPDs electrolytes exhibited inflection points at 2.44 V, whereas the inflection points of PAM-0.1CPDs, PAM-0.3CPDs, and PAM-0.5CPDs were located at 2.46, 2.56, and 2.48 V, respectively. These results indicate that the incorporation of CPDs can effectively suppress oxygen evolution reactions and broaden the electrochemical stability window of the electrolyte. Among all samples, PAM-0.3CPDs exhibited the highest decomposition voltage, demonstrating the most effective suppression of parasitic reactions. Subsequently, electrochemical impedance spectroscopy (EIS) measurements were conducted to investigate the ion transport behavior of the gel electrolytes with different CPDs contents. As shown in Fig. 6b, the charge-transfer resistance of the composite electrolytes was significantly lower than that of the pure PAM electrolyte, indicating that the incorporation of CPDs effectively facilitates Zn^{2+} transport kinetics and promotes rapid interfacial electrochemical reactions. Furthermore, the ionic conductivity of the gel electrolytes was evaluated based on the EIS results. As shown in Fig. 6c, the charge-transfer resistance initially decreased and then increased with increasing CPDs content. Correspondingly, the ionic conductivities of PAM, PAM-0.1CPDs, PAM-0.3CPDs, PAM-0.5CPDs, and PAM-0.7CPDs were calculated to be 10.4, 13.1, 38.6, 10.9, and 8.3 mS cm^{-1}, respectively, as summarized in Fig. 6d. Notably, PAM-0.3CPDs exhibited the highest ionic conductivity, further confirming that the optimized incorporation of CPDs significantly enhances ion transport kinetics within the hydrogel electrolyte.

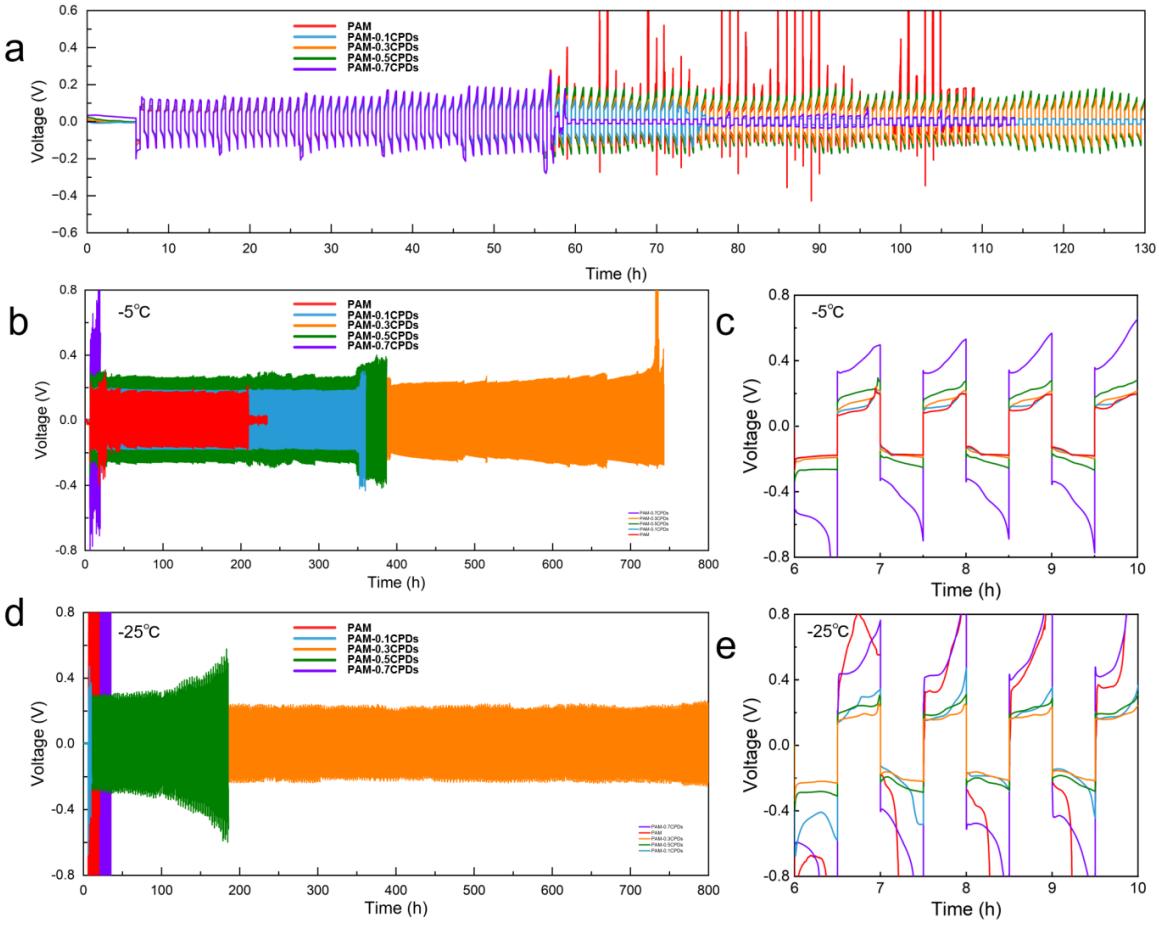

Figure 5 (a) Rate performance test curves of Zn||Zn symmetric batteries using gel electrolytes composed of various PAM formulations: PAM, PAM-0.1CPDs, PAM-0.3CPDs, PAM-0.5CPDs, and PAM-0.7CPDs; (b) Long-cycle performance test curves of the battery at-5℃; (c) Amplified view of the long-cycle performance test from 6 to 10 hours shown in (b); (d) Long-cycle performance test curves of the battery at-25℃; (e) Amplified view of the long-cycle performance test from 6 to 10 hours shown in (d).

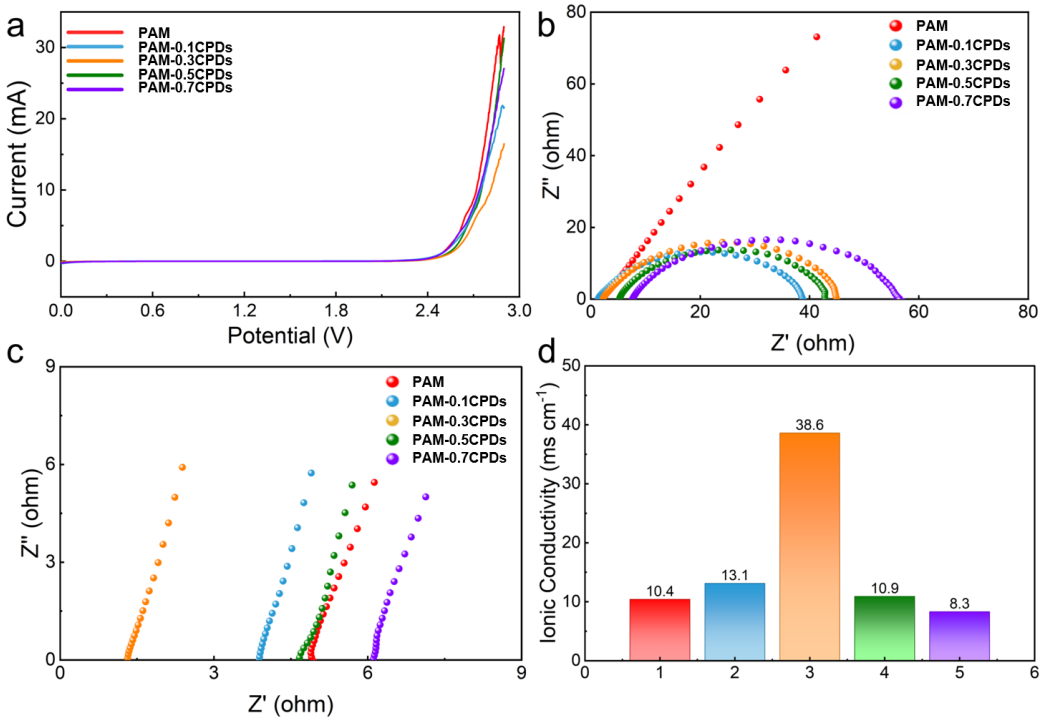

Figure 6 (a) linear sweep voltammetry (LSV) test, (b) Electrochemical impedance spectroscopy (EIS) test curves, (c) Ion conductivity test curves of Zn||Zn symmetric cells using the PAM, PAM-0.1CPDs, PAM-0.3CPDs, PAM-0.5CPDs, and PAM-0.7CPDs gel electrolytes; (d) Bar chart showing the ion conductivity values of each gel electrolyte.

4 Conclusion

In summary, a low-temperature composite hydrogel electrolyte based on polyacrylamide (PAM) and carbonized polymer dots (CPDs) was successfully constructed for high-performance aqueous zinc-ion batteries. Benefiting from the abundant hydroxyl and carboxyl functional groups on the CPDs surface, a multivalent hydrogen-bonding network was effectively established among CPDs, PAM chains, and water molecules, which significantly disrupted the hydrogen-bonding interactions of free water and promoted the conversion of free water into bound water. As a result, the freezing point of the hydrogel electrolyte was markedly reduced, while Zn^{2+} transport kinetics and interfacial stability were simultaneously improved under low-temperature conditions. Moreover, the incorporation of CPDs effectively regulated the Zn^{2+} solvation structure, suppressed hydrogen evolution side reactions and zinc dendrite growth, and enhanced the ionic conductivity of the electrolyte. Among all samples, PAM-0.3CPDs exhibited the optimal electrochemical performance, delivering stable cycling for 800 h at -25 ℃ under a current density of 2 mA cm^{-2} and an areal capacity of 1 mAh cm^{-2}. This work provides an effective strategy for the rational design of advanced low-temperature hydrogel electrolytes for high-performance aqueous zinc-ion batteries.

Acknowledgements: This work was supported by Jilin Province Science and Technology Development Plan Project (International cooperation 20240402073GH), the National Natural Science Foundation of China(22275030).

References

[1] Chen Jinhui, Tao Yingqing, Zhang Tianyu, et al.Toward durable wide-temperature Zn-MnO_2 batteries: A polarized dual-crosslinked hydrogel electrolyte for concurrent anode and cathode stabilization [J]. Chemical Engineering Journal, 2026(535):175539.

[2] Kang Jiahong, Wu Bozhi, Chen Shuning, et al. Solvent-induced biphasic phase separated hydrogels: Synergistic energy dissipation for softness, ultra-tough and shape recovery [J]. Chemical Engineering Journal, 2026(529):172732.

[3] Wu Yuying, Xie Dan, Liu Chang, Synergistic effect of hydrogen bond network and molecular cage enables wide-temperature quasi-solid zinc-ion batteries [J]. Chemical Engineering Journal, 2026(529):173033.

[4] Xiong Peixun, Kang Yingbo, Yao nan, et al. Zn-Ion Transporting, In Situ Formed Robust Solid Electrolyte Interphase for Stable Zinc Metal Anodes over a Wide Temperature Range [J]. ACS Energy Letters, 2023, 8 (3):1613–1625.

[5] Zhang Pengfei, Li Xinjie, Li Ziyue, et al. A highly stable zinc–air battery based on a non-alkaline agar gel electrolyte [J].

Energy & Environmental Science, 2026, 19 (3), 1069–1079.
[6] Gao Rui, Wang Jifeng, Song Yuanyuan, Polymer-Salt Effects with Enhanced Eutectic Behavior in Hydrogel Electrolytes for Aqueous Zinc Batteries at −70 ℃ [J]. Advanced Functional Materials, 2026,36 (2):e14585.
[7] Zhu Baonian, Yan Yuefeng, Hong Jingzhe, et al. Accelerated proton transport modulates dynamic hydrogen bonding networks in eutectic gel electrolytes for low-temperature aqueous Zn-metal batteries [J]. Journal of Energy Chemistry, 2025(109):325–336.
[8] Yang Ruiqiang, Zhang Yangqian, Liao Yaqi, et al. Double-network hybrid hydrogel electrolyte suppresses zinc dendrites and vanadium dissolution for durable zinc-metal batteries [J]. Energy Storage Materials, 2026(88):105097.
[9] Wu Runhai, Wang Ran, Yang Shaopei, et al. Bio-inspired hyaluronic acid enhanced dual-network hydrogel electrolyte unlocks dendrite-free Zn deposition and exceptional cycling stability in flexible zinc ion batteries [J]. Chemical Engineering Journal, 2026(530):173528.
[10] Liu Ziming, Zhang Xuke, Zhang Heng, et al. Construction of Homogeneously Porous Composite Hydrogel Electrolyte for Dendrite-Free Aqueous Zinc-Ion Batteries: An Alkali-Etched Graphitized-Carbon Nitride Induced Polymerization Strategy [J]. Advanced Functional Materials, 2026(0):e75312.
[11] Gou Lei, Zhu Lin, Wang Wei, et al. From Physical Cross-Linking to Tailored Phosphorylation: Unlocking High-Performance and Biocompatible Xanthan-Konjac Hydrogels for Zinc-Ion Batteries [J]. Advanced Materials, 2025, 37 (34):2505132.
[12] Lei Tongda, Wang Yongheng, Zhang Qingsong, et al. Ultra-stretchable and anti-freezing ionic conductive hydrogels as high performance strain sensors and flexible triboelectric nanogenerator in extreme environments [J]. Nano Energy, 2024(126):109633.
[13] Min Weixing, Li Lengwan, Wang Mingli, et al. Mastering the Copolymerization Behavior of Ethyl Cyanoacrylate as Gel Polymer Electrolyte for Lithium-metal Battery Application [J]. Angewandte Chemie International Edition, 2025, 64 (13):e202422510.
[14] Zhuang Wubin, Wang Zihan, Li Chaowei, et al. Acidic Hydrogel Enables Full-Period Mn^{2+}/MnO_2 Conversion in High-Energy Quasi-Solid-State Zn-MnO_2 Batteries [J]. Advanced Materials, 2026, 38 (13), e22827.
[15] Liu Ruiqi, Wan Fu, Liu Bowen, et al. A robust TPU/PVA semi-interpenetrating polymer network gel electrolyte enabling high-performance zinc-ion batteries [J]. Applied Surface Science, 2026(731):16441.
[16] Yan Yichen Duan Sidi, Liu Bo, et al. Tough Hydrogel Electrolytes for Anti-Freezing Zinc-Ion Batteries [J]. Advanced Materials, 2023, 35 (18):2211673.
[17] Zhao Wei, Zhang Yan, Liu Qingsong, et al. Entropy-Modulated Short-Chain Cathode for Low-Temperature All-Solid-State Li–S Batteries [J]. Angewandte Chemie International Edition, 2025, 64 (1):e202413670.
[18] Li Xiangye, Wang Dahui, Ran Fen, et al. Key approaches and challenges in fabricating advanced flexible zinc-ion batteries with functional hydrogel electrolytes [J]. Energy Storage Materials, 2023(56):351–393.
[19] Wang Zhenwu, Heck Matthias, Yang Wenwu, et al. Tough PEG gels by In Situ Phase Separation for 4D Printing [J]. Advanced Functional Materials 2024, 34 (20):2300947.
[20] Zheng Kun, Zhang Yang, Wang Jialin, et al. Custom hydrogen-bond network grants hydrogel superior zinc-anode stability [J]. Chemical Engineering Journal, 2026(530):173219.
[21] Li Tao, Liu Jiating, Shu Hang.et al. High-Performance Deep Eutectic/Ionic Liquid Gels for Zinc-Ion Battery and Flexible Sensor Applications in Extreme Environments [J]. Advanced Functional Materials, 2026,36 (3):e14358.
[22] Zhuang Wubin, Wang Zihan, Li Chaowei, et al. Acidic Hydrogel Enables Full-Period Mn^{2+}/MnO_2 Conversion in High-Energy Quasi-Solid-State Zn-MnO_2 Batteries [J]. Advanced Materials, 2026, 38 (13): e22827.